SolarPACES 2024, 30th International Conference on Concentrating Solar Power, Thermal, and Chemical Energy Systems

Solar Fuels and Chemical Commodities

https://doi.org/10.52825/solarpaces.v3i.2346

Published: 26 Jan. 2026

Analysis of Solar Heating Integration in a Liquid Metal Reactor for Hydrogen Production

Elisa Alonso[1], Luis F. González-Portillo[1], and Alberto Abánades[1]

[1]Universidad Politécnica de Madrid ETSII-UPM. Thermal Energy for Sustainability (TE4S) group. Madrid, Spain.

*Correspondence: Elisa Alonso, elisa.alonso@upm.es

Abstract. This study analyses the integration of concentrating solar energy with a liquid metal reactor for methane pyrolysis, configured as a vertical column. It compares two irradiation strategies: distributing radiation along the entire column height versus focusing it on the middle section. Parameters such as irradiance, total power, methane mass flow, and residence time are assessed. Both configurations present advantages and disadvantages, but designs achieving very high temperatures are preferred over those prioritizing thermal homogeneity. The findings provide insights for optimizing solar reactors for efficient hydrogen production.

Keywords: Solar Hydrogen, Solar Fuels, Heat Transfer Modelling

1. Introduction

Hydrogen is a potential contributor towards a sustainable future, serving not only as an alternative and non-polluting fuel for air, sea and land transportation as well as industry and buildings, but also as an energy carrier that enhances the dispatchability of renewable energy. Importantly, there are also several industry sectors for which hydrogen is a crucial feedstock [1]. However, from the sustainability point of view, the end-uses of hydrogen only will become truly meaningful if the hydrogen origin is clean and renewable.

Currently, 96% of hydrogen is produced from fossil fuels using thermal methods that result in CO_2/CO emissions. The main methods are steam reforming of natural gas, partial oxidation of hydrocarbons and coal gasification [2]. The remaining 4 % come from freshwater electrolysis which is still a very expensive (around 5 €/kg H_2) is associated with extensive water consumption and a requires the use of critical rare earth metals [3]. Methane pyrolysis, also known as methane cracking, is an alternative hydrogen production process that has been known since the 1960s. This process, which also produces high-value carbon black as a co-product, has been a subject of research interest ever since the 1980s and 1990s [4].

The process consists in dissociating the methane molecules (CH_4) into hydrogen (H_2) and high purity solid carbon (C) according to:

$$CH_4 \rightarrow C + 2H_2 \qquad \Delta H_{1273.15K} = 5673\ kJ/kg_{CH4} \tag{1}$$

A common issue that typically appears when the dissociation reaction is performed in gas-phase direct thermal reactors is carbon deposition on walls and ducts, leading to undesired blockages. Methane decomposition in liquid metal reaction media has been proposed as a potential alternative technology for practical industrial implementation. Its main advantage is a

simplified management of the carbon particles into the reactor via flotation: carbon black particles naturally rise to the top of the reactor owing to the difference in density with the liquid bath [5]. Carbon can then be mechanically recovered from the reactor top and exploited as a high-value co-product, thereby depositions and blockages are avoided. Performing the reaction in liquid metal effectively removes oxygen from the process without the need to use any ullage gas or vacuum. Moreover, the liquid metal bath facilitates the thermal management of the device, thanks to the high thermal conductivity of the reaction medium which leads to improved temperature homogeneity, fundamental for process scalability.

To ensure the sustainability of pyrolysis, the thermal energy source must be renewable. This study focuses on heating the pyrolysis reactor using concentrated solar energy. Extensive research has been conducted on solar reactors, exploring a lot of strategies for integrating solar heat with the reaction medium. This study compares two specific approaches to directing concentrated radiation onto the external wall of a ceramic column filled with liquid tin. In a real reactor, CH_4 would be bubbled through a diffuser at the bottom of the column, pass through the tin while heating up, and dissociate into H_2 and carbon. The first approach distributes the radiation evenly across the entire wall, while the second approach focuses the radiation on the middle third of the column height. The objective of this analysis is to determine whether the design of a concentrating system should favor a linear or point concentration geometry [6,7].

2. Reactor geometry and 2D thermal model

For this study, the reactor is simplified to a column shaped as a square-based prism. It is made of silicon carbide with a thickness of 2.5 cm. The inner dimensions are 15 x 15 x 60 cm. The top and bottom are closed with covers identical to the vertical walls. The reactor is insulated with 5 cm of insulation on all surfaces except the irradiated area. For simplification, the entire volume of the column is considered to be filled with liquid tin. The reactor is placed outdoors with ambient and sky temperature equal to 25 ºC. Figure 1 shows the geometry and boundary conditions used in the 2D model. A negative volumetric power is considered in the tin domain to account for the reaction enthalpy of methane dissociation into hydrogen. As this parameter depends on the introduced methane mass flow, a range of values is examined. Different solar power values and irradiances are also assessed.

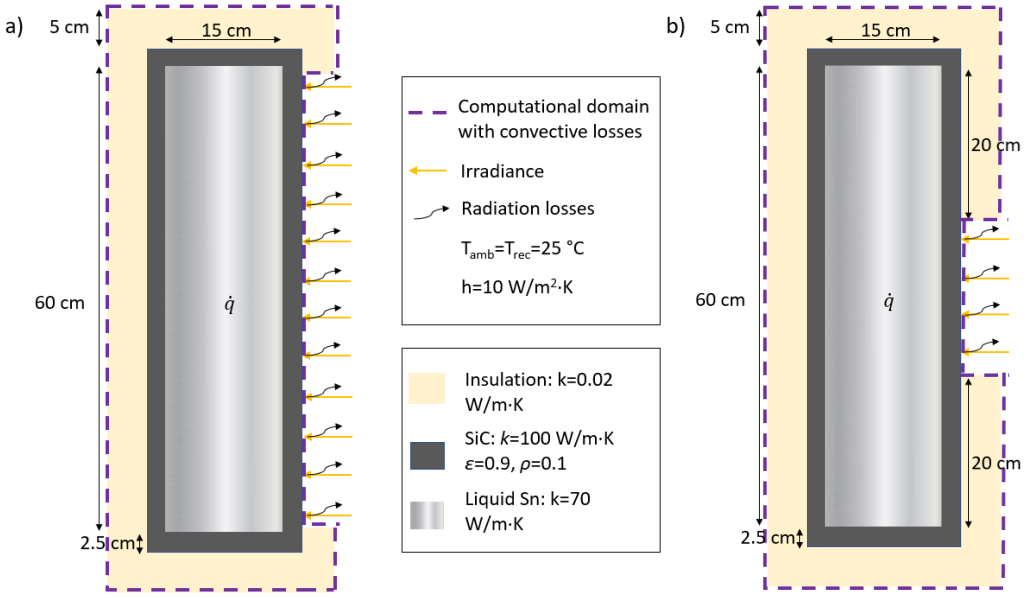

Figure 1. *Geometry and boundary conditions used in the 2D model. (a) Solar irradiance impinging on the entire wall. (b) Solar irradiance impinging on the middle third of the wall.*

Fixed values have been selected por materials properties and convection coefficient for natural convection in air, as indicated in Figure 1. At steady state, equations governing the heat transfer in each part and boundary of the reactor are the following:

Tin: $$\frac{\partial^2 T}{\partial x^2} + \frac{\partial^2 T}{\partial z^2} + \frac{\dot{q}}{k_{tin}} = 0 \quad (2)$$

Silicon carbide: $$k_{SiC}\left(\frac{\partial^2 T}{\partial x^2} + \frac{\partial^2 T}{\partial z^2}\right) = 0 \quad (3)$$

Insulation: $$k_{ins}\left(\frac{\partial^2 T}{\partial x^2} + \frac{\partial^2 T}{\partial z^2}\right) = 0 \quad (4)$$

Non-irradiated boundary: $$k_{ins}\left(\frac{\partial T}{\partial x} + \frac{\partial T}{\partial z}\right) + h(T - T_{amb}) = 0 \quad (5)$$

Irradiated boundary (assuming grey surface):

$$k_{SiC}\left(\frac{\partial T}{\partial x} + \frac{\partial T}{\partial z}\right) + \rho G + \varepsilon \cdot \sigma \cdot \left(T^4 - T_{sky}^4\right) + h(T - T_{amb}) = 0 \quad (6)$$

Equations 2 to 6 have been discretized to apply the finite-difference method and solved in every node of a 0.0025 m side mesh.

Although the gas flow is not simulated in this model, a term for consumed power due to the hydrogen production, $\dot{q}$, is computed as:

$$\dot{q} = \frac{4 \cdot \Delta H_r \cdot \dot{m}_{H2}}{V_r} \quad (7)$$

where ΔH_r is the reaction enthalpy of (1), V_r is the reactor volume and $\dot{m}_{H2}$ the mass flow of produced hydrogen.

Generated hydrogen depends on the CH_4 mass flow and its conversion into H_2. To estimate it, a first order kinetic mechanism is assumed, according to most of the literature findings, and the Arrehious equation is applied to relate the reaction rate with the temperature. Activation energy and preexponetial factor are included in such equation as an average of a set of previosly published values , which are showed in *Table 1*.

Table 1. *Kinetic data for CH_4 thermal dissociation reported by different authors. Data and references are compiled in* [8].

Author and year	A(s^{-1})	E_a (kJ/mol)
Napier and Subrahmanyam, 1972	$3.8 \cdot 10^{13}$	392
Olsvik et al., 1995	$1 \cdot 10^{13}$	366
Abanades and Flamant, 2006, 2007	$5 \cdot 10^{13}$	350
Patrianakos et al., 2011	$1 \cdot 10^{14}$	400
Rodat et al., 2009	$6.6 \cdot 10^{13}$	370
Average	$5.3 \cdot 10^{13}$	375

Therefore, the reaction velocity for each node of the discretized tin domain, *i*, is estimated as:

$$r_i = k \cdot [CH_4] = A \cdot e^{\frac{-E_a}{R \cdot T_i}} \cdot [CH_4]_i \quad (8)$$

and assuming $[CH_4]_i = 1$ for simplification. Although it is expected that, in this system, every single bubble flowing in the liquid tin behaves as a batch mini-reactor, the simplication is adopted in order to evaluate the velocity dependence with temperature.

Then, for a given residence time, which can be set and tuned during the detailed design process,τ_r, the mass flow of generated hydrogen is:

$$\dot{m}_{H2} = \frac{\dot{m}_{CH4} \cdot \tau_r \cdot \sum_1^N r_i}{N \cdot 4} \quad (9)$$

where $\dot{m}_{CH4}$ is the mass flow of methane introduced into the reactor and *N* the total numer of mesh nodes corresponding to the tin. According to the model formulation, conversion from CH_4 to H_2 will be complete when $\tau_r \cdot \sum_1^N r_i \geq 1$, which may not reproduce real condition but it is first approach for the current parametric analysis. Therefore, upper limit for operation parameters have been fixed in those values that lead to 100 % of methane conversion according to the results presented below.

Conversion of methane, χ, which can be defined as the ratio of transformed methane mols to the initial methane moles, assuming all the consumed methane is converted into H_2, is calculated according to Equation 10.

$$\chi = \frac{2 \cdot \dot{m}_{H2} \cdot PM_{CH4}}{PM_{H2} \cdot \dot{m}_{CH4}} \quad (10)$$

The two geometrical configurations for the solar reactor showed in Figure 1, case-1 and case-2, have been modeled and the parametric values compiled in Table 2 have been evaluated for each one. Studied cases are denomined with a letter from A to N and each one has been defined with radiative boundary conditions that lead to temperature range compatible with methane pyrolysis.

Table 2. *Studied cases and values of the considered parameters.*

	Case-1 (G on the entire wall. Area: 0.12 m^2)			
A	Reference case			
	Irradiance, G (kW/m^2)	150		
	Power, q=G·A (kW)	18		
	(kg/s)$\dot{m}_{CH4}$	$4{\cdot}10^{-4}$		
B,C,D	Different irradiance			
	Irradiance, G (kW/m^2)	100	175	190
	Power, q=G·A (kW)	12	21	22.8
	(kg/s)$\dot{m}_{CH4}$	$4{\cdot}10^{-4}$	$4{\cdot}10^{-4}$	$4{\cdot}10^{-4}$
E, F, G	Different methane mass flow			
	Irradiance, G (kW/m^2)	150	150	150
	Power, q=G·A (kW)	18	18	18
	(kg/s)$\dot{m}_{CH4}$	$1.2{\cdot}10^{-4}$	$2{\cdot}10^{-4}$	$5{\cdot}10^{-4}$
	Case-2 (G on a third of wall. Area: 0.04 m^2)			
H	Reference case			
	Irradiance, G (kW/m^2)	300		
	Power, q=G·A (kW)	12		
	(kg/s)$\dot{m}_{CH4}$	$4{\cdot}10^{-4}$		
I, J, K	Different irradiance			
	Irradiance, G (kW/m^2)	250	325	327
	Power, q=G·A (kW)	10	13	13.1
	(kg/s)$\dot{m}_{CH4}$	$4{\cdot}10^{-4}$	$4{\cdot}10^{-4}$	$4{\cdot}10^{-4}$
L, M, N	Different methane mass flow			
	Irradiance, G (kW/m^2)	300	300	300
	Power, q=G·A (kW)	12	12	12
	(kg/s)$\dot{m}_{CH4}$	$3.4{\cdot}10^{-4}$	$3.7{\cdot}10^{-4}$	$5{\cdot}10^{-4}$

Additionally, it is studied how the conversion is affected by residence time, defined as the average time elapsed since the CH_4 molecules enter and leave the liquid tin. For fixed total power of 12 kW and $\dot{m}_{CH4}$ of $3.4{\cdot}10^{-4}$ kg/s, residence times leading to conversions ranging from 0.1% to 100% have been obtained for both cases 1 and 2. These specific power and mass flow values were selected to facilitate a comparison of the residence times required for the two irradiation configurations under study. Nevertheless, the parametric analysis results indicate that each configuration operates optimally within distinct parametric ranges.

3. Results

Temperatures of reference cases 1 and 2 are shown in Figure 2 in the form of colored contour intervals. Note that the figure represents a complete rectangular section including the zone free from insulation where the radiation impinges on the column wall. Therefore, the deeper blue color corresponds to the ambient air surrounding the solar concentration area, which has not been modeled but appears in the figures. According to nomenclature in Table 2, Figure 2 features studied cases A and H. Total power is higher for case-1 (A) but higher maximum temperature is achieved in 2 (H). Lowest minimum tin temperature also corresponds to case-2, particularly around the top and bottom, because thermal gradients are higher as the radiation is concentrated on a smaller area of the reactor wall.

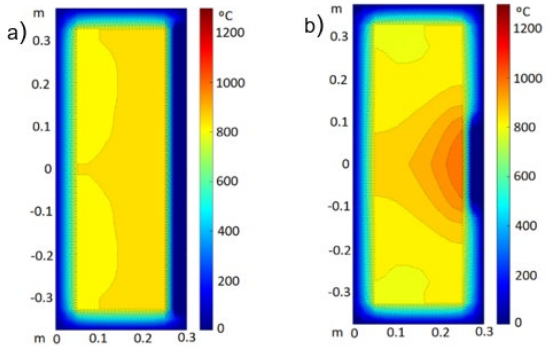

Figure 2. *Temperature distribution for the two reference cases (A and H). (a) Solar irradiance impinging on the entire wall (case-1 configuration). (b) Solar irradiance impinging on the middle third of the wall (case-2 configuration).*

Figures 3, 4 and 5 correspond to the parametric analysis performed with the model. In Figure 3, the conversion of methane is represented for cases A, B, C and D and H, I, J and K.

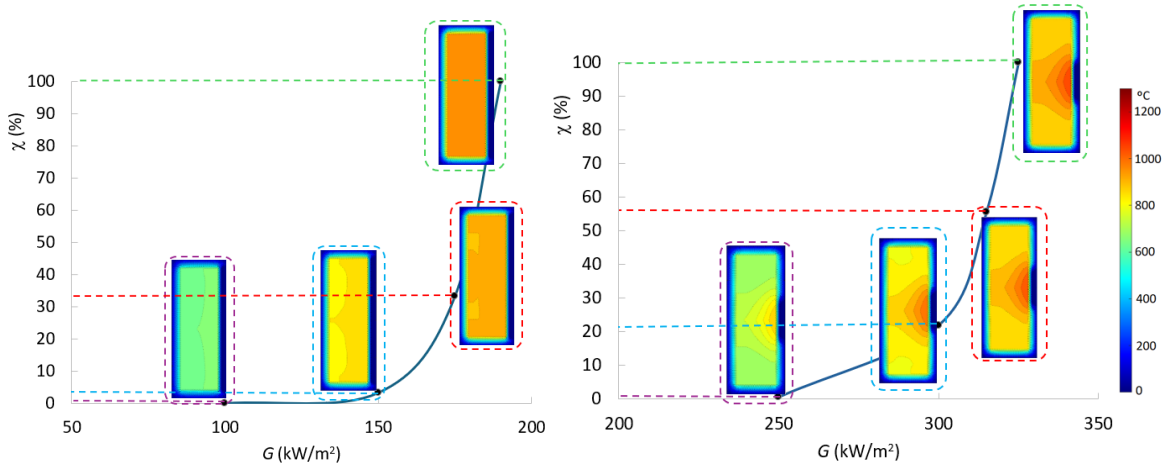

Figure 3. *Methane conversion for different irradiances. Left: case 1, where radiation impinges on the entire wall and right: case 2, with radiation concentrated on a third of the column wall. Figure includes sections of the reactor with colored maps of temperatures for informative purposes. Color legend is valid for both graphs.*

Figure 3 represents the influence of irradiance on methane conversion, which is dependent on the tin temperature and thus the reaction temperature. The mass flow of methane and the residence time are invariable for all four cases represented in each graph. Consistently, the higher the irradiance, the higher the conversion, with this effect being more pronounced when radiation impacts one third of the column wall (case-1). To achieve complete conversion, the required uniform irradiance must be over 1.7 times higher in case-2 than in case-1. However, when evaluating total power on the irradiated wall area instead of irradiance, these results are reversed.

Figure 4 shows the relationship between methane conversion and the mass flow introduced into the reactor, with constant irradiance and residence time maintained in each case. The methane mass flow reduces the tin temperature as it absorbs heat to dissociate into H_2 and C. Consequently, a lower mass flow results in a higher temperature and increased conversion.

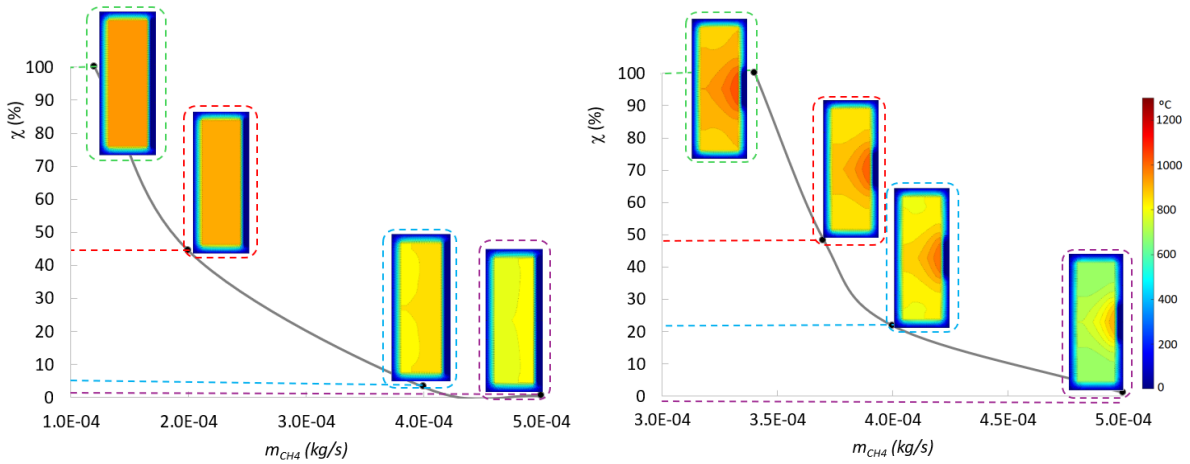

Figure 4. *Methane conversion for different inlet methane mass flow. Left: case-1, where radiation impinges on the entire wall and right: case-2, with radiation concentrated on a third of the column wall. Figure includes sections of the reactor with colored maps of temperatures for informative purposes. Color legend is valid for both graphs.*

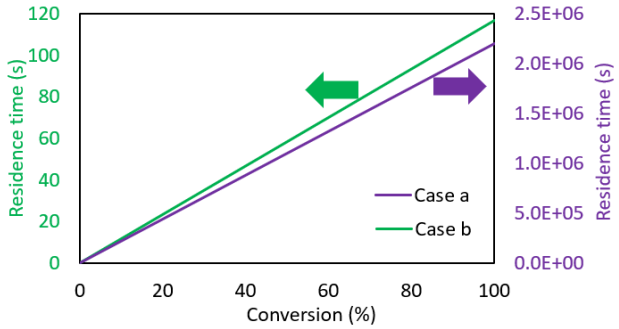

Figure 5. *Residence time versus conversion of methane for cases 1 and 2 operation under the same total power (12 kW) and methane mass flow ($3.4 \cdot 10^{-4}$ kg/s).*

According to equations 9 and 10, residence time will influence conversion directly and proportionally, provided that the reaction temperature and reaction velocity remain constant. Figure 5 compares the evolution of conversion with residence time for configurations 1 and 2, operating under the same total power and methane mass flow. The residence time for case-1 is six orders of magnitude greater than for case-2, due to the parameters for the former being out of design. To operate with reasonable residence times, the case-1 configuration must be designed for higher total power and lower irradiance, within the range of values included in *Table 2*.

Consistent with the Arrhenius equation, the results demonstrate that for a given residence time, the reaction rate depends exponentially on the reaction temperature. In the case-2 configuration, despite the thermal non-uniformity, the hotter zones in the tin promote rapid conversion. On the other hand, thermal uniformity alone does not significantly enhance methane conversion, as the absence of very hot regions leads to slower reaction kinetics.

4. Conclusions and key insights for reactor and concentration system design

Configurations 1 and 2 could approach a linear and a point focus solar concentration system. To the question, "Which configuration is better?", Figure 6 provides insights inferred from the 2D thermal model and the subsequent parametric analysis. The blue boxes on the left include aspects concerning the design of the reactor and concentration system for solar pyrolysis of

CH_4 bubbled in liquid tin. Each configuration entails advantages and disadvantages; however, within the range of temperatures viable for pyrolysis, results show benefits for H_2 production when operating at the upper extreme.

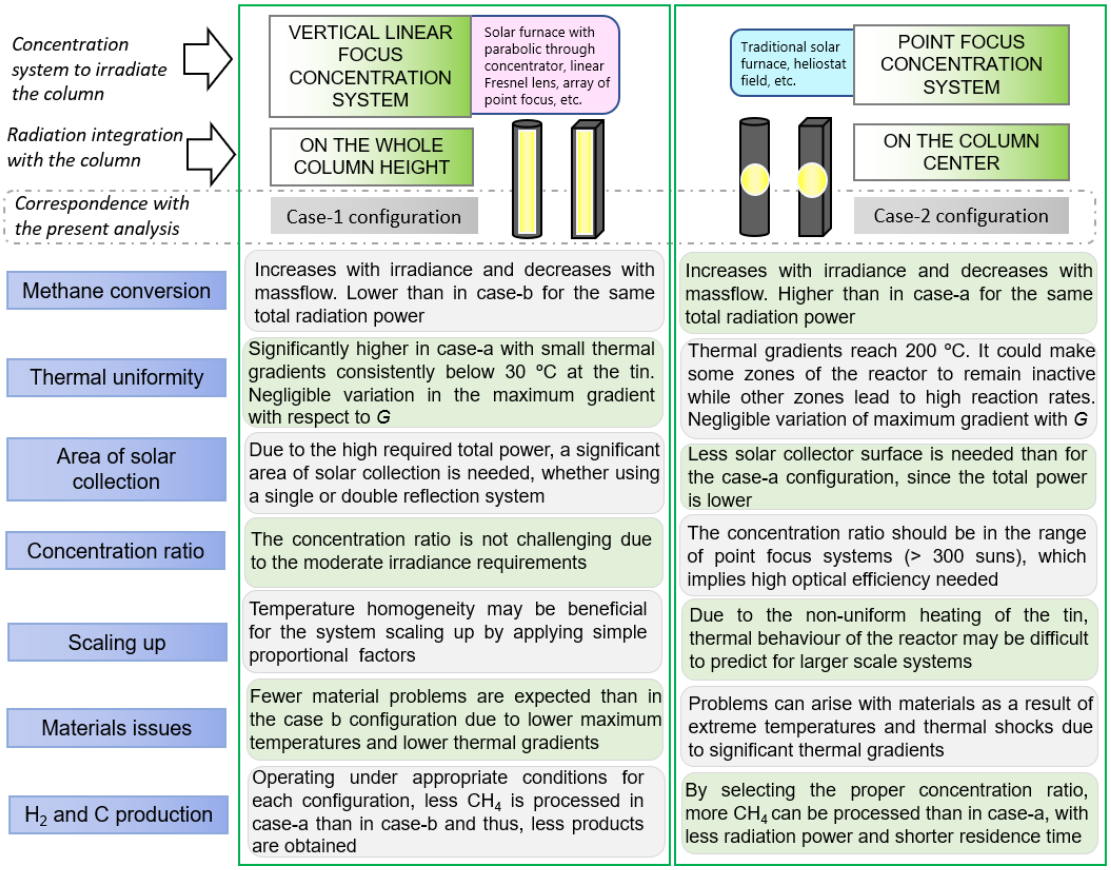

Figure 6. *Summary of the conclusions in the form of key insights for a further design and construction of a solar pyrolysis reactor and a concentration system*

Author contributions

E. Alonso: conceptualization, data curation, formal analysis, investigation, methodology, writing-original draft.

L.F. González-Portillo: investigation, writing-review&editing.

A. Abánades: conceptualization, funding acquisition, investigation, writing-review&editing.

Competing interests

The authors declare that they have no competing interests.

Acknowledgement

This work has been carried out within the BrainEn Missions project with exp. MIG-20211033 in the framework of the Recovery, Transformation and Resilience funded by CDTI. This research has been partialy supported by the Spanish Ministerio de Ciencia e Innovación under the project of reference number PID2023-151272OA-I00.

References

[1] Hydrogen Council, Path to hydrogen competitiveness: a cost perspective, 2020. www.hydrogencouncil.com.
[2] I.D. Muhammed Iberia Aydin, An assessment study on various clean hydrogen production methods, Energy. 245 (2022) 123090. https://doi.org/10.1016/j.energy.2021.123090.
[3] M. Msheik, S. Rodat, S. Abanades, Methane cracking for hydrogen production: A review of catalytic and molten media pyrolysis, Energies. 14 (2021). https://doi.org/10.3390/en14113107.
[4] C.H. Steinberg M, Modern and Prospective Technologies for Hydrogen Production from Fossil Fuels., Int. J. Hydrog. Energy,. 14 (1989) 797-820. https://doi.org/https://doi.org/10.1016/0360-3199(89)90018-9.
[5] S. Postels, A. Abánades, N. von der Assen, R.K. Rathnam, S. Stückrad, A. Bardow, Life cycle assessment of hydrogen production by thermal cracking of methane based on liquid-metal technology, Int. J. Hydrogen Energy. 41 (2016) 23204–23212. https://doi.org/10.1016/j.ijhydene.2016.09.167.
[6] M.S. Reyhaneh Loni, Performance comparison of a solar parabolic trough concentrator using different shapes of linear cavity receiver, Case Stud. Therm. Eng. 60 (2024) 104603. https://doi.org/10.1016/j.csite.2024.104603.
[7] H. González-Caramillo, A. Gallo, I. Padilla, C.A. Pérez-Rábago, C.-A. Asselineau, M. Romero, A. López-Delgado, Design solutions and characterization of small scale and very high concentration furnace using a Fresnel lens, Appled Therm. Eng. 255 (2024) 124044. https://doi.org/https://doi.org/10.1016/j.applthermaleng.2024.124044.
[8] T. Becker, M. Richter, D.W. Agar, Methane pyrolysis: Kinetic studies and mechanical removal of carbon deposits in reactors of different materials, Int. J. Hydrogen Energy. 48 (2023) 2112–2129. https://doi.org/10.1016/j.ijhydene.2022.10.069.